Pegylated IFN-α regulates hepatic gene expression through transient Jak/STAT activation

Michael T. Dill,[1,2] Zuzanna Makowska,[1] Gaia Trincucci,[1] Andreas J. Gruber,[3] Julia E. Vogt,[4] Magdalena Filipowicz,[1,2] Diego Calabrese,[1] Ilona Krol,[1] Daryl T. Lau,[5] Luigi Terracciano,[6] Erik van Nimwegen,[3] Volker Roth,[4] and Markus H. Heim[1,2]

[1]Department of Biomedicine, Hepatology Laboratory, University of Basel, Basel, Switzerland. [2]Division of Gastroenterology and Hepatology, University Hospital Basel, Basel, Switzerland. [3]Biozentrum, University of Basel and Swiss Institute of Bioinformatics, Basel, Switzerland. [4]Computer Science Department, University of Basel, Basel, Switzerland. [5]Liver Center, Department of Medicine, Beth Israel Deaconess Medical Center, Harvard Medical School, Boston, Massachusetts, USA. [6]Institute of Pathology, University Hospital Basel, Basel, Switzerland.

The use of pegylated interferon-α (pegIFN-α) has replaced unmodified recombinant IFN-α for the treatment of chronic viral hepatitis. While the superior antiviral efficacy of pegIFN-α is generally attributed to improved pharmacokinetic properties, the pharmacodynamic effects of pegIFN-α in the liver have not been studied. Here, we analyzed pegIFN-α–induced signaling and gene regulation in paired liver biopsies obtained prior to treatment and during the first week following pegIFN-α injection in 18 patients with chronic hepatitis C. Despite sustained high concentrations of pegIFN-α in serum, the Jak/STAT pathway was activated in hepatocytes only on the first day after pegIFN-α administration. Evaluation of liver biopsies revealed that pegIFN-α induces hundreds of genes that can be classified into four clusters based on different temporal expression profiles. In all clusters, gene transcription was mainly driven by IFN-stimulated gene factor 3 (ISGF3). Compared with conventional IFN-α therapy, pegIFN-α induced a broader spectrum of gene expression, including many genes involved in cellular immunity. IFN-induced secondary transcription factors did not result in additional waves of gene expression. Our data indicate that the superior antiviral efficacy of pegIFN-α is not the result of prolonged Jak/STAT pathway activation in hepatocytes, but rather is due to induction of additional genes that are involved in cellular immune responses.

Introduction

Interferons (IFNs) are central mediators of immune responses to viral infections (1). They exert their antiviral activity by inducing the expression of hundreds of genes that together establish an "antiviral state," which restricts the spread of virus among neighboring cells (2). Type I IFNs (all IFN-αs and IFN-β) bind to the IFN-α receptor (IFNAR) and activate the receptor-associated tyrosine kinases Jak1 and Tyk2, which in turn activate signal transducer and activator of transcription 1 (STAT1) and STAT2 by phosphorylation of a tyrosine in the C-terminal domain (3). Activated STAT1 combines with STAT2 and IFN regulatory factor 9 (IRF9) to form IFN-stimulated gene factor 3 (ISGF3). ISGF3 translocates into the nucleus, binds to IFN-stimulated response elements (ISREs) in gene promoters and induces the transcription of hundreds of genes. Activated STAT1 can also form homodimers that bind to γ-activated sequences (GASs) and induce an overlapping but distinct set of IFN-stimulated genes (ISGs). IFN-induced Jak/STAT signaling is tightly controlled by negative regulators. Suppressor of cytokine signaling 1 (SOCS1) and SOCS3 are rapidly induced and strongly inhibit STAT1 phosphorylation at the receptor-kinase complex within hours (4). SOCS proteins are also rapidly degraded and in most cells become undetectable within hours after their induction. However, IFN signaling remains refractory for days in many cell types (5). In the liver of mice repeatedly injected with IFN-α, a long-lasting upregulation of ubiquitin-specific peptidase 18 (USP18) was found to be responsible for prolonged unresponsiveness of liver cells to IFN-α (6).

For more than 25 years, recombinant IFN-α has been used for the treatment of hepatitis C virus (HCV) infections (7). HCV is a parenterally transmitted positive-strand RNA virus that replicates in human hepatocytes and can cause chronic hepatitis with progressive fibrosis, leading to cirrhosis and hepatocellular carcinoma (8). Initially, unmodified recombinant IFN-α2a or -α2b was used alone or in combination with the antiviral compound ribavirin. In 2001, pegylated IFN-α (pegIFN-α) became the standard of care because of its superior efficacy (9, 10). The covalent attachment of polyethylene glycol (PEG) molecules to IFN-α produces a biologically active molecule with a longer half-life. The delayed clearance allows once-weekly injections, compared with three times a week for conventional IFN-α. It is generally assumed that the sustained high serum concentrations of pegIFN-α provide for uninterrupted antiviral activity through a permanent stimulation of the IFN signaling pathways, whereas the serum concentrations of standard IFN-α (with an elimination half-life of 4 to 10 hours) decline below pharmacologically active levels in the second half of each 48-hour dosing interval (11, 12). However, there is no experimental evidence supporting prolonged pharmacodynamic effects of pegIFN-α. On the contrary, the refractoriness of Jak/STAT signaling in mouse liver challenges the concept that pegIFN-α is more effective because of prolonged stimulation of IFN signaling pathways (6).

We previously investigated pegIFN-α–induced signaling and gene regulation in the liver of 16 patients who started treatment of their chronic hepatitis C (CHC) (13). All patients had a pre-

Conflict of interest: The authors have declared that no conflict of interest exists.
Citation for this article: *J Clin Invest.* 2014;124(4):1568–1581. doi:10.1172/JCI70408.

treatment liver biopsy during the routine work-up for CHC and a second liver biopsy 4 hours after the first subcutaneous injection of pegIFN-α. Six patients had an induction of ISGs already before treatment and showed no further activation of IFN signal transduction or ISG expression in response to pegIFN-α. None of these patients responded to therapy (13). It is now firmly established that patients with an activated endogenous IFN system are poor responders to IFN-α–based therapies (13–16), and quantification of the expression of a limited number of ISGs from liver biopsies allows the most accurate prediction of response to pegIFN-α and ribavirin (17). In the 10 patients without a preactivation of the hepatic IFN system, pegIFN-α induced phosphorylation and nuclear translocation of STAT1 and the expression of hundreds of ISGs within 4 hours (13). Nine patients had a sustained virological response (SVR) later and were cured of CHC, and 1 patient had a virological response during treatment, but later relapsed.

In the present work, again using a paired biopsy approach, we extended the pharmacodynamic analysis of pegIFN-α to the entire 1-week dosing interval in an additional 12 patients. Three patients each had a second liver biopsy 16, 48, 96, and 144 hours after the first injection of pegIFN-α2b. This unique analysis of the molecular effects of pegIFN-α in human liver revealed that Jak/STAT signaling occurs in the first 24 hours and then becomes refractory in hepatocytes for the entire dosing interval despite persistently high pegIFN-α serum concentrations. Compared with conventional IFN-α, we found that pegIFN-α induced a broader spectrum of ISGs, including many genes involved in cellular immune responses. The initial activation of ISGF3 was the main driver of ISG transcription during the entire week after the first injection of pegIFN-α. The induction of secondary transcription factors and of unphosphorylated STAT1 (U-STAT1) had negligible effects. We conclude that the superior therapeutic efficacy of pegIFN-α is not caused by a sustained activation of the Jak/STAT pathway in hepatocytes, but rather by the sustained induction of ISGs in liver-infiltrating immune cells.

Results

pegIFN-α2b induced STAT1 phosphorylation and ISG expression in the liver. We studied pegIFN-α2b–induced STAT1 phosphorylation and gene regulation in 18 patients who underwent treatment for CHC with pegIFN-α and ribavirin. All patients had a first liver biopsy before treatment during the routine clinical CHC work-up. A second biopsy was taken 4 hours (n = 6), 16 hours (n = 3), 2 days (n = 3), 4 days (n = 3), and 6 days (n = 3) after the first injection of pegIFN-α2b. The 6 patients whose second liver biopsy was performed 4 hours after injection were selected from among the 16 patients who had already been included in the previous study described above (13), because they had no preactivation of the endogenous IFN system in the liver and a normal response to pegIFN-α2b. The patients were selected in a two-step procedure for the later time points. First, liver biopsies from patients with CHC who agreed to donate part of their liver biopsy for research were analyzed with a previously developed and validated four-gene classifier to predict their likelihood of responding to pegIFN-α (17). Patients with a high probability of an unimpaired, normal response to pegIFN-α were then asked to participate in our study and to consent to a second liver biopsy. This two-step selection process was necessary, because in patients with preinduced hepatic ISGs, the Jak/STAT signaling pathway is refractory in liver cells (13), and a second liver biopsy would have been of little use for the study of pegIFN-α pharmacodynamic effects in the liver. Indeed, the selection process with the four-gene classifier was highly accurate in predicting a good response to pegIFN-α: all patients were treatment responders, and apart from 1 patient who relapsed after treatment, all patients were cured of their HCV infection (Table 1).

We analyzed pegIFN-α2b–induced Jak/STAT signaling by immunohistochemistry (IHC) with phosphorylated STAT1–specific (p-STAT–specific) antibodies. Because we selectively included only patients who had no pretreatment induction of the endogenous IFN system, STAT1 was not activated in the biopsies obtained before treatment (Figure 1A). Following the first pegIFN-α2b injection, we observed a rapid and strong activation of STAT1 already 4 hours later, with nuclear p-STAT1 signals detected in more than 60% of hepatocytes (Figure 1). p-STAT1 signals were still strong after 16 hours, but then rapidly declined. In liver biopsies obtained after 2, 4, or 6 days, p-STAT1 signals in hepatocytes were weak and were detected in less than 5% of hepatocytes. In nonparenchymal cells, we detected p-STAT1 signals at all time points.

To further address the kinetics of ISG induction by pegIFN-α2b, we adapted a highly sensitive and specific in situ hybridization (ISH) method (QuantiGene ViewRNA) that allowed the detection of ISG mRNAs in fresh-frozen liver biopsy samples. We detected *MX1* mRNA already 4 hours after the injection of pegIFN-α2b and found that it peaked at the 16-hour time point and then rapidly declined (Figure 2A). *IFI27* mRNA expression peaked at 16 hours and declined at a much slower rate. Of note, the intensity of the signals declined in all hepatocytes, and at later time points we did not detect hepatocytes with the signal intensities found at the 16-hour point. Together with the absence of strong nuclear p-STAT1 signals in hepatocytes at later time points (Figure 1A), these data do not support the hypothesis that hepatocytes recover asynchronously from the refractory state and that they are, in part, restimulated by pegIFN-α2b circulating at high concentrations during the entire dosing interval (Table 1).

In contrast to hepatocytes, we found that nonparenchymal cells showed strong nuclear p-STAT1 signals also at later time points (Figure 1A, arrows). Accordingly, *SOCS1* and *PDL1* mRNAs, two ISGs that are only transiently induced in hepatocytes, were also expressed at the 144-hour time point in nonparenchymal cells (Figure 2B).

We conclude that in hepatocytes, pegIFN-α2b induces a transient activation of the Jak/STAT signaling pathway during the first day, but not during the entire 1-week dosing interval, and this despite sustained high serum concentrations of pegIFN-α2b at all time points (Table 1). We found that nonparenchymal cells remained IFN-α sensitive at all time points investigated.

Induction of negative regulators of Jak/STAT signaling. We then assessed the induction of negative regulators of IFN signaling in the liver biopsies. On the mRNA level, *SOCS1* was strongly induced at 4 hours and 16 hours, but then returned to pretreatment expression levels (Figure 3A). SOCS3 was also upregulated in the first 16 hours, albeit to a lesser extent (up to 2.5-fold) and remained slightly elevated for up to 4 days. USP18 was also rapidly induced, but unlike SOCS1 and SOCS3, the expression level of *USP18* mRNA remained persistently high during the entire week (Figure 3A). Accordingly, USP18 protein was detectable from 16 hours on at all time points by Western blot and IHC analyses (Figure 3, B and C). Presumably for technical reasons, we could not detect SOCS1 or SOCS3 proteins at any time point, despite testing several different antibodies.

Table 1
Patient characteristics

Patient no.	Age (yr)	Sex	HCV GT	Viral load, log IU/ml			Response			METAVIR	IL28B GT	Time point	Medication	IFN conc pg/ml
				Baseline	4-wk	12-wk	4-wk	12-wk	Follow-up					
1	52	M	3	7.14	Neg	Neg	RVR	cEVR	SVR	A2/F2	CC	4 h	pegIFN-α2b	138
2	37	M	3	4.9	Neg	Neg	RVR	cEVR	SVR	A1/F2	CT	4 h	pegIFN-α2b	530
3	54	F	2	4.95	Neg	Neg	RVR	cEVR	SVR	A3/F3	CT	4 h	pegIFN-α2b	214
4	57	M	3	5.25	2.15	Neg	Non-RVR	cEVR	Relapse	A3/F4	CC	4 h	pegIFN-α2b	702
5	38	M	4	4.08	1.66	Neg	Non-RVR	cEVR	SVR	A2/F2	CT	4 h	pegIFN-α2b	241
6	51	F	1	6.82	3.52	Neg	Non-RVR	cEVR	SVR	A1/F2	CT	4 h	pegIFN-α2b	419
7	26	M	3	4.58	Neg	Neg	RVR	cEVR	SVR	A1/F1	TT	16 h	pegIFN-α2b	1,194
8	42	F	3	5.49	Neg	Neg	RVR	cEVR	SVR	A1/F2	CT	16 h	pegIFN-α2b	774
9	41	M	3	5.66	Neg	Neg	RVR	cEVR	SVR	A1/F2	CT	16 h	pegIFN-α2b	973
10	30	M	3	7.07	Neg	Neg	RVR	cEVR	SVR	A2/F2	CT	48 h	pegIFN-α2b	356
11	57	F	1	5.95	Neg	Neg	RVR	cEVR	SVR	A2/F2	CC	48 h	pegIFN-α2b	414
12	37	M	3	6.72	1.28	Neg	Non-RVR	cEVR	SVR	A3/F2	CT	48 h	pegIFN-α2b	887
13	62	M	4	7.16	Neg	Neg	RVR	cEVR	SVR	A3/F4	CT	96 h	pegIFN-α2b	1,567
14	43	M	1	5.6	1.63	Neg	Non-RVR	cEVR	SVR	A3/F2	CC	96 h	pegIFN-α2b	155
15	40	M	1	5.16	1.41	Neg	Non-RVR	cEVR	SVR	A3/F4	CT	96 h	pegIFN-α2b	186
16	25	F	1	2.64	Neg	Neg	RVR	cEVR	SVR	A2/F2	CC	144 h	pegIFN-α2b	NA
17	70	M	2	6.86	1.84	Neg	Non-RVR	cEVR	SVR	A2/F3	CT	144 h	pegIFN-α2b	NA
18	34	M	3	5.56	Neg	Neg	RVR	cEVR	SVR	A2/F2	CT	144 h	pegIFN-α2b	233
19	57	F	2	5.18	Neg	Neg	RVR	cEVR	SVR	A2/F2	CC	144 h	pegIFN-α2a	6,564
20	57	M	1	6.54	4.59	3.33	Non-RVR	EVR	Interrupted	A3/F4	CT	144 h	pegIFN-α2a	6,146
21	38	F	4	6.32	5.07	Neg	Non-RVR	cEVR	SVR	A3/F4	CC	144 h	pegIFN-α2a	15,986

conc, concentration; GT, genotype; Neg, negative; RVR, rapid virological response (undetectable viral load at 4 weeks); cEVR, complete early virological response (undetectable viral load at 12 weeks); EVR, early virological response (>$\log_2$ reduction of viral load at 12 weeks); SVR, sustained virological response (undetectable viral load 24 weeks after end of treatment); METAVIR, liver histology score for grading inflammation (A1–A3) and staging fibrosis (F0–F4).

We conclude that pegIFN-α2b induces transient activation of the Jak/STAT signaling pathway in hepatocytes because of the rapid induction of SOCS1, SOCS3, and USP18 and that the signaling pathway remains refractory to ongoing stimulation by circulating pegIFN-α2b because of the persistent induction of USP18.

pegIFN-α2b–induced genes fall into four robust classes with distinct temporal expression patterns. We assessed pegIFN-α2b–regulated gene expression with transcriptome analysis using Affymetrix U133 Plus 2.0 arrays. Pairwise comparison of pretreatment and on-treatment biopsies revealed a greater than 2-fold induction in two-thirds of samples of hundreds of genes, with a peak at 16 hours (Figure 4A and Supplemental Table 1; supplemental material available online with this article; doi:10.1172/JCI70408DS1). Likewise, up to 200 genes were downregulated (Supplemental Table 2). To gain insight into the temporal expression patterns of ISGs induced by pegIFN-α2b in the human liver, we analyzed the transcriptome data using a Bayesian clustering algorithm. The algorithm produced four robust clusters of upregulated genes, which were termed early (144 genes), intermediate (31 genes), late (299 genes), and very late ISGs (20 genes) (Figure 4B and Supplemental Table 1). For over 95% of all upregulated genes, the peak mRNA levels occurred 4 or 16 hours after injection, followed by a steady decline over the remaining 128 hours of treatment (Figure 4B). Because of the limited amount of tissue obtained by percutaneous liver biopsies, we could not comprehensively analyze ISG protein expression. We therefore measured the protein expression of three exemplary ISGs. USP18 protein expression peaked at the 16-hour time point and then gradually declined, but remained induced up to the 144-hour time point. We found that *USP18* mRNA expression peaked already at 4 hours, but was also persistently induced up to the 144-hour time point (Figure 3). *STAT1* mRNA was induced up to the 96-hour time point, whereas STAT1 protein expression was still increased at 144 hours (Supplemental Figure 1). We found a very good correlation between *IP10* mRNA expression in the liver and IP-10 protein concentration in the serum (Supplemental Figure 1). Taken together, we found a reasonably good correlation between mRNA and protein expression of ISGs in this limited set of exemplary ISGs.

Compared with conventional IFN-α, pegIFN-α2b induces a broader range of genes including many ISGs involved in cellular immune responses. Given the known superior antiviral efficacy of pegIFN-α, we could not treat our study patients with conventional IFN-α. To compare IFN-α and pegIFN-α–induced gene regulation, we therefore made use of previously published transcriptome data obtained 24 hours after the injection of conventional IFN-α (18). Fortunately, the samples were analyzed on the same Affymetrix U133 Plus 2.0 arrays, allowing a direct comparison of the data. The discrepant time points after injection between the pegIFN-α and the IFN-α studies were a potential pitfall, but unsupervised hierarchical clustering of the combined data positioned the IFN-α2a samples properly between the 16-hour time point and the 48-hour time point of the pegIFN-α samples. Importantly, the magnitude of mRNA upregulation in the IFN-α samples was comparable to that in the pegIFN-α samples from the 16- and 48-hour time points. The most striking difference between IFN-α and pegIFN-α was the number of genes that were induced more than 2-fold in two-thirds of the samples (Figure 5A). We found that most of the genes upregulated by IFN-α were also

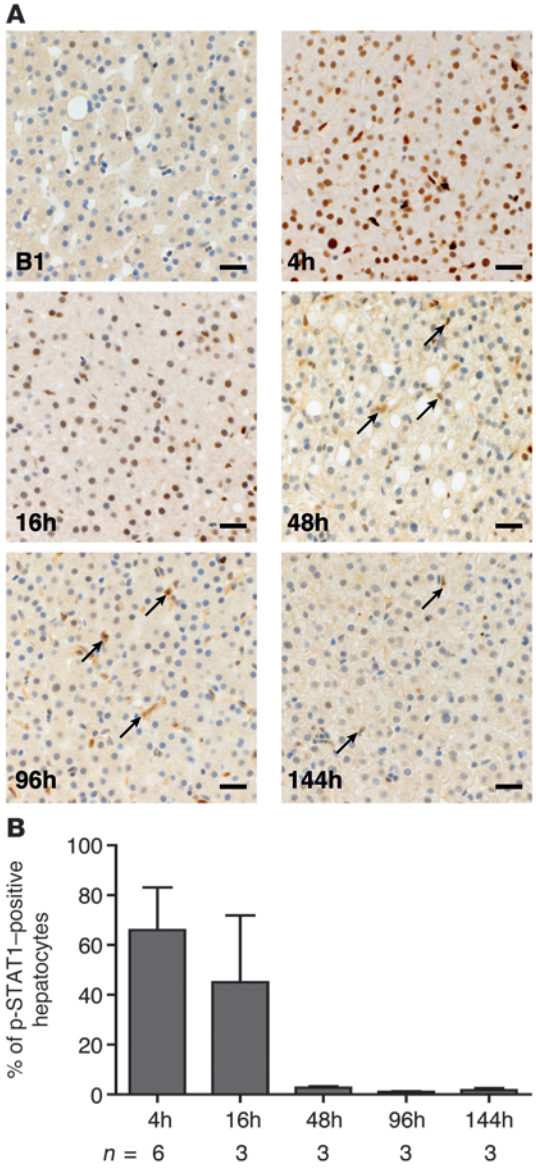

Figure 1
pegIFN-α2b transiently induces the Jak/STAT pathway in the liver. (**A**) Representative images of IHC analysis of p-STAT1 in liver biopsies obtained before treatment (B1) and at several time points after the first injection of pegIFN-α2b. Strong nuclear p-STAT1 signals were present at the 4- and 16-hour time points, but not at later time points, where the signals were localized in nonparenchymal cells (arrows). Scale bars: 20 μm. (**B**) Quantitative analysis of the mean percentage of p-STAT1–positive hepatocyte nuclei (5 × 100 cells counted per sample; the number of samples is indicated) per time point. Bars show the mean with SEM.

induced by pegIFN-α, but a substantially larger number of genes were induced more than 2-fold exclusively by pegIFN-α. Gene ontological (GO) analysis revealed these to be genes associated with immune cells and adaptive immunity, whereas the genes upregulated by both IFN-α and pegIFN-α fell into the "classical" ISG group (Figure 5, B and C, and Supplemental Table 4). We conclude that while a common subset of ISGs is upregulated within the first 1–2 days independently of the IFN-α formulation, an additional set of genes associated with cellular immune responses is more markedly induced by pegIFN-α.

pegIFN-α2a and pegIFN-α2b induce overlapping sets of genes in the liver 144 hours after injection despite their different pharmacokinetic properties. Two different formulations of pegIFN-α2 with distinct pharmacokinetic properties are approved for the treatment of viral hepatitis: pegIFN-α2b (PegIntron) and pegIFN-α2a (PEGASYS). While the single-chain PEG moiety of pegIFN-α2b is subject to hydrolysis, which leads to release of IFN-α2b into the human body and faster elimination of the drug, pegIFN-α2a is not hydrolyzed, has a lower absorption rate, and is eliminated at a much slower rate (19). pegIFN-α2a achieves maximal serum levels of 7,000 pg/ml about 80 hours after administration, and the peak extends up to 168 hours after injection (20), as opposed to a much earlier peak (15–44 hours) and a more rapid decline of pegIFN-α2b. In order to investigate whether these distinct pharmacokinetic properties result in distinct pharmacodynamic effects, we included 3 additional patients in our study who were treated with pegIFN-α2a and obtained a second liver biopsy at the end of the 1-week dosing interval. As expected, pegIFN-α2a serum concentrations were still high at the end of the first week, whereas pegIFN-α2b concentrations declined in the second half of the dosing interval (Table 1). However, despite the difference in serum concentration between pegIFN-α2a and pegIFN-α2b, we found that the number of genes upregulated by greater than 2-fold in two-thirds of the patients in each group was not significantly different (59 versus 49 genes, respectively). Furthermore, we observed a considerable overlap of the gene sets, with 26 genes being upregulated by both pegIFN-α2a and pegIFN-α2b, and these common genes comprised most of the typical ISGs (Supplemental Table 3). We conclude that the different pharmacokinetic properties of the two pegIFN-α2 formulations do not cause significant differences in ISG expression at the end of a 1-week dosing interval.

pegIFN-α2b–induced gene transcription is mainly driven by IFN-stimulated response element motifs during the entire dosing interval. Among the hundreds of genes induced by IFN-α, one also finds several transcription factors such as IFN regulatory factors (IRFs) and cytokines and chemokines that could directly or indirectly activate additional signal transduction pathways and transcriptional programs (Supplemental Table 1). Such "secondary" transcription factors could be the drivers of gene transcription at later time points when pegIFN-α2b–induced Jak/STAT signaling is refractory. We therefore analyzed the relative contribution of transcription factor–binding motifs to global gene expression at 4 hours, 16 hours, 2 days, 4 days, and 6 days using a recently developed method called motif activity response analysis (MARA) (21). MARA infers the activities of transcription regulators by modeling genome-wide expression profiles in terms of computationally predicted binding sites for a large array of mammalian regulatory motifs such as IFN-stimulated response element (ISRE). Roughly speaking, MARA infers that a regulatory motif increases in activity when its predicted target promoters show an overall increase in expression that cannot be explained by the occurrence of other regulatory motifs in these promoters. In our current application, we used MARA to calculate changes in the activity of motifs across paired samples (pretreatment versus on-treatment). This analysis revealed ISRE as the most substantially changing motif across all time points up to 6 days (Figure 6, A and B). We observed a strong positive ISRE motif activity change in all patients (Figure 6A). MARA identified additional motifs that contribute to gene expression changes such as GAS,

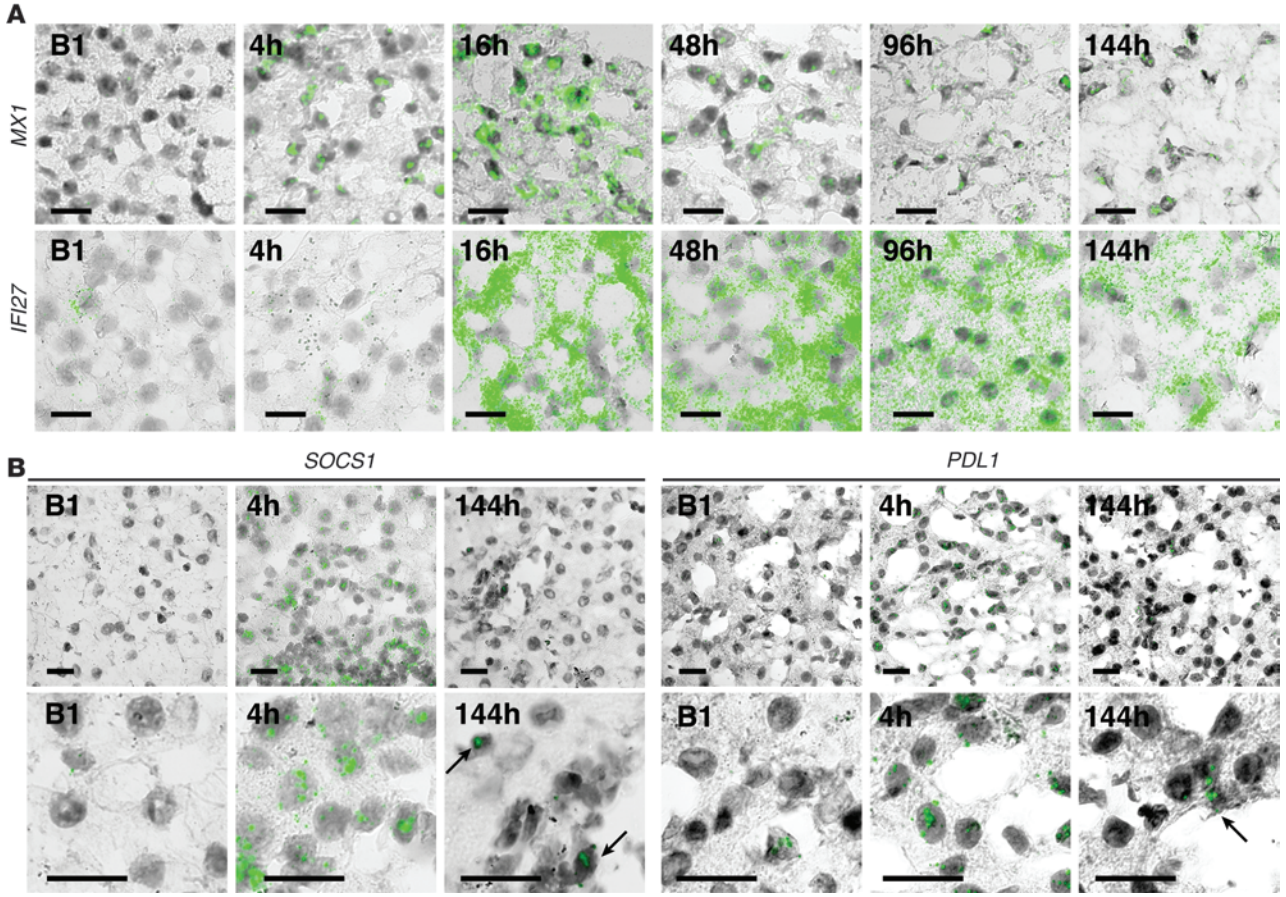

Figure 2
ISH reveals distinct expression patterns of ISG mRNAs at different time points. (**A**) Representative examples of ISH staining (green) in liver biopsies for *MX1* and *IFI27* mRNA showing that ubiquitous expression gradually declined over time with distinct kinetics. (**B**) ISH staining (green) in liver biopsies for *SOCS1* and *PDL1* mRNA revealed expression in hepatocytes and in nonparenchymal cells at 4 hours. At 144 hours, SOCS1 and PDL1 were detected only in nonparenchymal cells (black arrows). Scale bars: 20 μm.

DMAP1_NCOR{1,2}_SMARC (DMAP1), PRRX1,2, and ATF6. However, the changes in their activities were relatively minor in comparison with ISRE (Figure 6B). MARA results of the transcription factor–binding site (TFBS) analysis were confirmed by motif discovery analysis using HOMER software (22). In each of the four ISG clusters (Figure 4B), ISRE was by far the most significantly enriched motif (Supplemental Figure 2).

ISRE motifs are the binding sites for ISGF3 and also IRFs. ISGF3 is activated by IFN-α–induced phosphorylation of STAT1 and STAT2. IRFs are transcriptionally induced and are also regulated by phosphorylation (23). We therefore measured the expression of IRF mRNAs. Of the nine IRFs, only *IRF1*, *IRF7*, and *IRF9* were upregulated by pegIFN-α2b in the liver (Figure 6C). IRF1 is transiently induced at the 4- and 16-hour time points. IRF9 is part of the ISGF3 complex, and its transcriptional activity depends on p-STAT1 and p-STAT2. IRF7 is upregulated during the entire dosing interval of pegIFN-α2b and could also be involved in ISRE-mediated gene transcription. However, the transcriptional activity of IRF7 depends on serine phosphorylation by IKK-α (24), a downstream component of cellular sensory pathways that are activated by viral pathogen–associated molecular patterns (PAMPs).

Unphosphorylated STAT1 does not prolong ISG induction. The central IFN-α–induced signal transducer and transcription factor STAT1 is itself one of the most strongly induced ISGs. Indeed, we found *STAT1* mRNA strongly induced in the first 4 days after pegIFN-α2b injection (Supplemental Table 1). STAT1 protein was even upregulated during the entire 1-week dosing interval (Supplemental Figure 1). The functional significance of the expression of large amounts of U-STAT1 protein is unclear, but, intriguingly, a recent paper described a role of U-STAT1 as an active transcription factor that prolongs gene transcription after dephosphorylation of p-STAT1 (25). In that work, thirty ISGs were found to be upregulated by U-STAT1–driven transcription (25). We therefore hypothesized that U-STAT1 could be involved in the prolonged ISG induction by pegIFN-α2b. However, when we took the list of U-STAT1–induced genes and investigated their expression during the first week of pegIFN-α2b therapy, we did not find them to be overrepresented in clusters 3 and 4 with late and very late induced ISGs, respectively (data not shown). We therefore decided to address the potential of U-STAT1 to induce gene transcription in a more rigorous way. To that end, STAT1-deficient U3A cells (26) were stably transfected with STAT1 wild-type (STAT1-WT) or a mutant STAT1 with a phos-

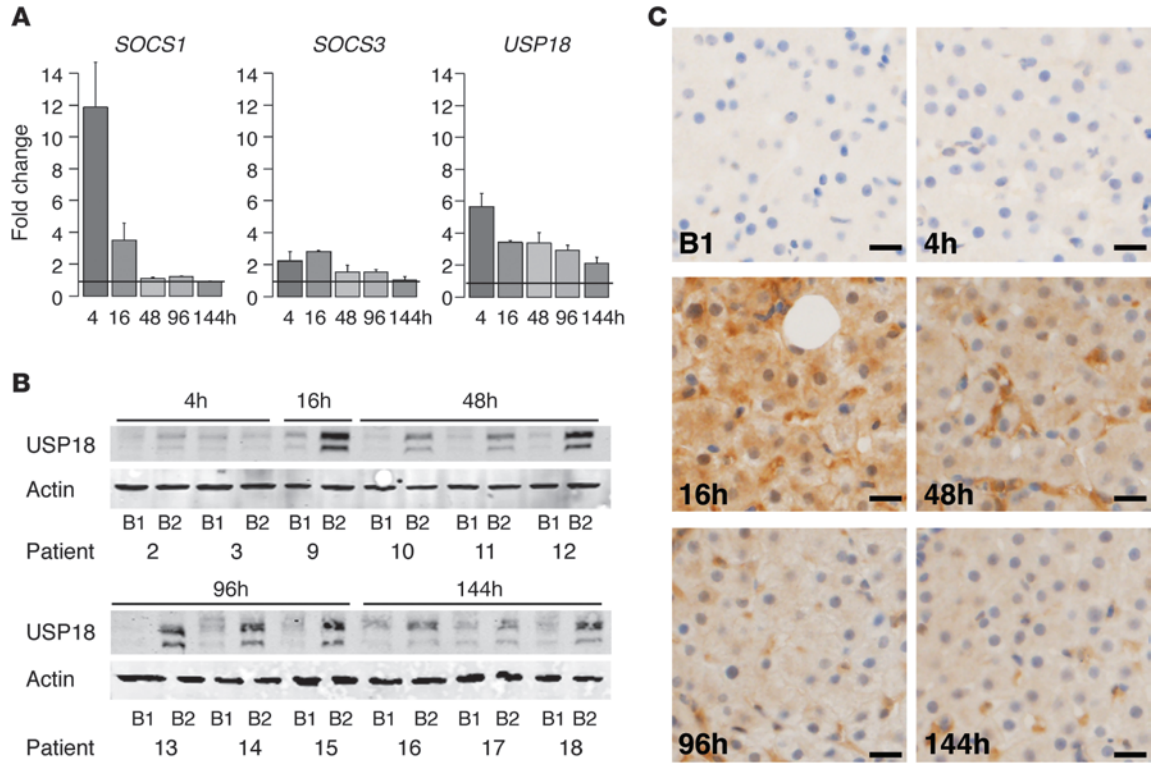

Figure 3

The negative regulator USP18 is continuously upregulated during the entire week after pegIFN-α2b injection. (**A**) Bar plot indicating the mRNA expression fold change between the pretreatment biopsy (B1) and the on-treatment biopsy (B2) of *SOCS1*, *SOCS3*, and *USP18*. Data represent the mean with SEM ($n = 6$ for the 4-hour time point; $n = 3$ for all other time points). The black line indicates the baseline measured in pretreatment biopsies from the same patients ($n = 18$). (**B**) USP18 protein expression by Western blot analysis using whole-cell extracts of liver samples from B1 and B2. Patients are numbered according to Table 1. (**C**) Representative images of IHC for USP18 of liver biopsies obtained before treatment (B1) and at several time points after the first injection of pegIFN-α2b as indicated. Scale bars: 20 μm.

pho-tyrosine acceptor site at position 701 mutated to phenylalanine (STAT1-Y701F). For both STAT1-WT and STAT1-Y701F, three clones with different STAT1 expression levels were selected. One clone each expressed the transfected STAT1 at levels usually present in unstimulated parental 2fTGH cells, one clone each expressed the constructs at levels found after maximal STAT1 expression obtained in 2fTGH cells stimulated with IFN-α for 24 hours, and one clone each expressed the transfected constructs at intermediate levels (Figure 7A). As we expected, IFN-α treatment of U3A cells transfected with STAT1-WT induced ISGs. In contrast, we observed no ISG induction in U3A cells transfected with STAT1-Y701F (Figure 7B and Supplemental Figure 3). These results do not support a role for U-STAT1 in prolonged ISG expression.

Ongoing gene transcription and lower mRNA decay rates both contribute to prolonged expression of "late" ISGs. Since ISRE seems to be the main TFBS in all transcription clusters and U-STAT1 was not able to induce ISGs, we next hypothesized that the genes belonging to the late ISG clusters might show prolonged expression due to lower mRNA degradation rates, since such a mechanism was recently proposed to play an important role in temporal expression patterns of genes induced by TNF-α (27). Decay of mRNAs can be regulated by specific microRNA recognition sequences present in the 3′ untranslated regions (UTRs) of mRNAs (28). We therefore analyzed our transcriptome datasets for specific binding sites of microRNAs to test whether the four ISG clusters defined by our unbiased clustering approach (Figure 4) have distinct microRNA binding sites in their 3′UTRs. However, we could not identify biologically meaningful microRNA binding patterns that would predict or explain the differences in decay rates of the four clusters (data not shown). We also analyzed the decay rates of mRNAs experimentally in IFN-α–treated Huh7 cells by inhibition of gene transcription with actinomycin D. Relative to *GAPDH* mRNA, early ISGs (*RSAD2*, *USP18*) showed faster mRNA decay, while the late ISGs (*IFI27*, *LGALS3BP*) decayed more slowly than *GAPDH* (Figure 8A). However, a delayed mRNA decay rate cannot readily explain the expression peaks at later time points such as those observed in cluster 4 genes (Figure 3). We therefore also analyzed the transcription of representative early (*RSAD2*, *USP18*) and late (*IFI27*, *LGALS3BP*) ISGs using a nuclear run-on assay. Nuclei were isolated from Huh7 cells after 1, 2, 4, 16, and 24 hours of stimulation with 1,000 IU/ml IFN-α and were then incubated with biotin-labeled UTP for 45 minutes. The newly transcribed mRNA was purified on streptavidin beads and quantified by quantitative PCR (qPCR). We found a markedly prolonged transcription of late versus early ISGs (Figure 8B).

We conclude that the temporal expression patterns of ISGs are determined by the duration of gene transcription as well as by different mRNA decay rates.

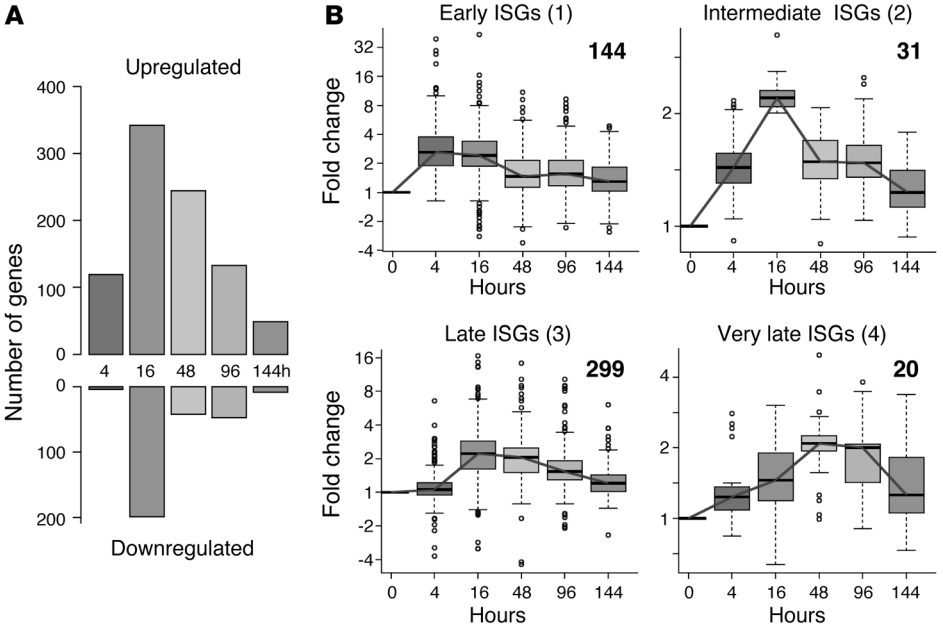

Figure 4
pegIFN-α2b–induced genes fall into four robust classes with distinct temporal expression patterns. (**A**) Number of genes greater than 2-fold up- or downregulated in two-thirds of the patients at each time point. (**B**) Clustering analysis of the upregulated genes produced four robust clusters (numbers 1–4) composed of early, intermediate, late, and very late ISGs. Boxes represent the quartiles, and whiskers represent 1.5 times the interquartile range. Bold line indicates the median expression value, and the number of genes in each cluster is indicated.

Discussion

Arguably, no other cytokine has been used in clinical medicine more extensively than recombinant (peg)IFN-α. Hundreds of thousands of patients with chronic hepatitis B and CHC have been treated worldwide in the past 20 years. Despite this clinical success story, amazingly little is known about the mechanism of action and the pharmacodynamic effects of IFN-α and pegIFN-α. In principle, IFN-α exerts its antiviral effect both through the induction of antiviral effector systems in infected cells and through the regulation of immune cells such as natural killer cells, dendritic cells, and T cells (1). Immunomodulatory effects of IFN-α have been investigated in cells isolated from blood in patients with CHC undergoing therapies with (peg)IFN-α. Indeed, several studies reported that HCV-specific T cell reactivity is increased by IFN-α treatment and correlates with treatment response (29–31). However, other investigators have shown no association (32, 33). The direct effects of (peg)IFN-α on hepatocytes are more difficult to study because of the requirement of liver biopsies from patients undergoing pegIFN-α treatments. In a previous study including 16 patients with CHC, we analyzed pegIFN-α2b–induced Jak/STAT signaling and global gene expression in paired liver biopsies obtained before treatment and 4 hours after the first injection of pegIFN-α2b (13). Unexpectedly, in 6 patients we found an upregulation of hundreds of ISGs already in pretreatment biopsies. In these "preactivated" patients, we found no significant further increase in the number or expression level of ISGs induced by pegIFN-α2b and no increase in the p-STAT1 nuclear signal intensity. Apparently, the constitutive activation of the endogenous IFN system not only fails to eliminate the virus, but also inhibits Jak/STAT signaling and thereby inhibits a response to pegIFN-α2b treatments (13). In a follow-up study, we developed and validated a classifier based on the expression of four genes in the liver that allows one to predict a response to (peg)IFN-α in individual patients (17). In the present study, we made use of this classifier to screen patients with CHC and included 12 patients who did not have an activated endogenous IFN system in the liver. This selection process allowed us to exclude patients with refractory Jak/STAT signaling pathways. The results from our present study most likely reflect IFN responses in general, because the patients with CHC who were included had normal responsiveness of IFN-α signaling pathways in the liver.

Ever since the introduction of pegIFN-α into therapeutic regimens for CHC, the prevailing explanation for the superior efficacy of pegIFN-α compared with that of conventional IFN-α was centered on the prolonged high serum concentration of pegIFN-α molecules. In this paradigm, the permanently high serum levels of pegIFN-α were equated with a permanent stimulation of the target cells, i.e., the infected hepatocytes. The inferior efficacy of IFN-α was explained by the short serum half-life that caused serum levels to return to baseline in the second half of the 2-day dosing interval, leaving the infected hepatocytes unstimulated and thereby enabling a periodic resurgence of HCV replication. Based on the results of our present study, we refute this model. Our data show an activation of the Jak/STAT pathway in the liver only during the first day, despite prolonged high serum concentrations of pegIFN-α2b. This finding is in agreement with experimental data from studies in chimpanzees that showed only transient induction of ISGs after pegIFN-α2a injection (34). The molecular mechanisms that temporally limit IFN-α signaling most likely involve two negative regulators of IFN-α–induced Jak/STAT signaling. We observed in our study that within hours after pegIFN-α2b injection, SOCS1 and USP18 were induced in the liver, and USP18 remained strongly upregulated during the entire 1-week dosing interval. Solid evidence from experiments with genetically modified mice shows that SOCS1 and USP18 have a central role in inhibiting IFN-α–induced Jak/STAT signaling (6, 35, 36). We therefore conclude that SOCS1 and USP18 upregulation in the liver of patients treated with pegIFN-α2b restricts Jak/STAT signaling during the first day of the 1-week dosing interval.

This conclusion is further supported by the fact that we did not observe a significant increase in the number or the expression level of ISGs induced at the 144-hour time point in patients treated

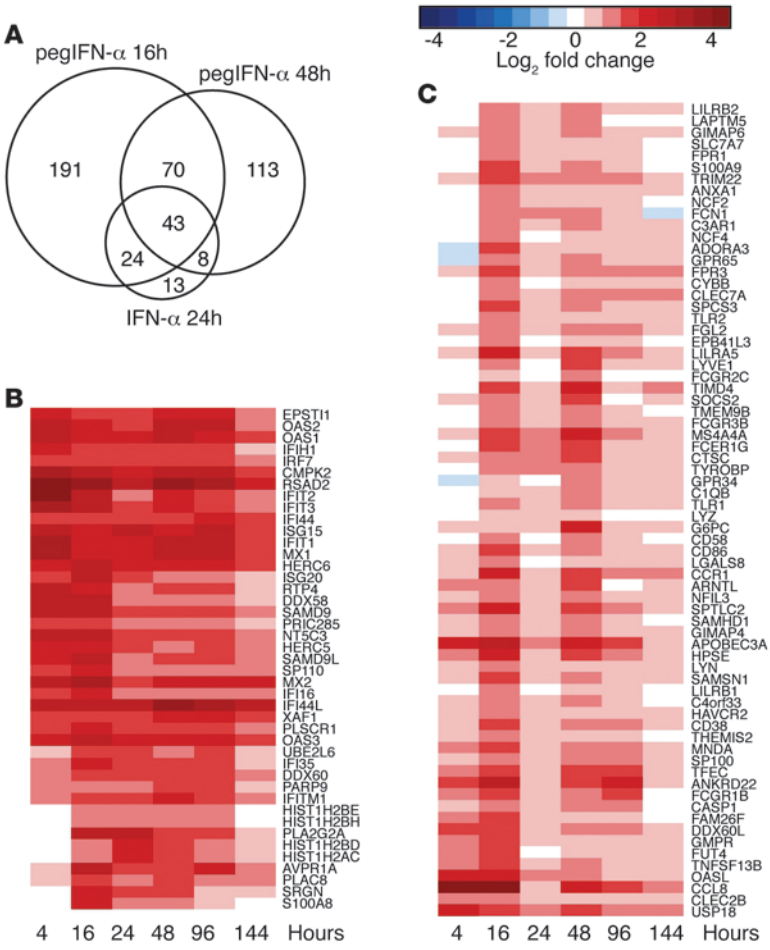

Figure 5
IFN-α2a induces mainly "classical" ISGs, while pegIFN-α2b leads to transcription of additional immune cell–associated genes. (**A**) Venn diagram of genes identified as being upregulated by more than 2-fold in two-thirds of the patients at 16 or 48 hours after pegIFN-α2b injection (n = 3 each) or 24 hours after conventional IFN-α injection (n = 6). (**B** and **C**) Heatmaps show expression patterns (mean $\log_2$ fold change compared with paired pretreatment biopsies) of genes upregulated after IFN-α injection. (**B**) 43 ISGs were upregulated by conventional IFN-α2a at 24 hours as well as by pegIFN-α2b at both 16 and 48 hours. (**C**) 70 ISGs were upregulated by pegIFN-α2b at both 16 and 48 hours, but not by conventional IFN-α2a at 24 hours.

with pegIFN-α2a compared with those treated with pegIFN-α2b, despite the high serum concentrations of pegIFN-α2a in all 3 patients. The refractoriness of Jak/STAT signaling pathways in the liver apparently overrides the potential benefits of the prolonged serum half-life of pegIFN-α2a. Indeed, in a large clinical study, pegIFN-α2a had no superior antiviral efficacy compared with that of pegIFN-α2b (37). Taken together, the assumption that increasing the serum half-life of IFN-α formulations necessarily improves their antiviral efficacy because of an uninterrupted stimulation of IFN-α responses in hepatocytes cannot be sustained. The comparison of the gene sets induced by conventional IFN-α versus pegIFN-α supports a different mechanism: pegIFN-α induces a more sustained upregulation of a set of genes involved in cellular immune responses. The superior antiviral efficacy is most likely caused by an increased stimulation of the cellular immune response to HCV. It remains to be clarified which immune cells are critically involved in pegIFN-α–induced antiviral activities. It also remains to be clarified why pegIFN-α can induce this broader set of genes. For the 75 genes found in the intersection of conventional and pegIFN-α (Figure 5A), the magnitude of mRNA expression and the fold induction over baseline were equal for both IFN-α and pegIFN-α. Therefore, for the induction of those classical ISGs in hepatocytes, IFN-α is not less potent compared with pegIFN-α. However, IFN-α's short half-life of 6 to 8 hours might become important for nonparenchymal cells, i.e., liver-resident immune cells that were found to be responsive to pegIFN-α during the entire week after pegIFN-α injection. Based on our data, we propose a model in which the superior antiviral efficacy of pegIFN-α is the result of continuous stimulation of immune cells and is not due to continuous stimulation of the Jak/STAT pathway in HCV-infected hepatocytes.

A large body of fundamental knowledge about the key signaling pathways and the biological role of IFN-α has been acquired through cell culture experiments and mouse models with genetic deletions of IFNs, IFN receptors, or components of the Jak/STAT pathway (38). On the other hand, the IFN-α–induced effects in target organs of human pathogens have been little investigated. Not surprisingly, the molecular mechanisms responsible for the antiviral activity of (peg)IFN-α against HCV are still not known. In the Huh7 cell–based HCV replicon system, overexpression and siRNA interference screens identified several ISGs involved in the inhibition of replication, among them: *IRF1*, *IRF2*, *IRF7*, IFN-induced helicase C domain–containing protein 1 (*IFIH1*, also known as *MDA5*), retinoic acid–inducible gene 1 (*RIGI*, also known as *DDX58*), mitogen-activated protein kinase kinase kinase 14 (*MAP3K14*), IFN-induced protein with tetratricopeptide repeats 3 (*IFIT3*), IFN-induced transmembrane protein 1 (*IFITM1*), *IFITM3*, phospholipid scramblase 1 (*PLSCR1*), *TRIM14*, *RNASEL*, and inducible nitric oxide synthase (*INOS*, also known as *NOS2*) (39, 40). With the exception of *MAP3K14* and *NOS2*, all of these ISGs were indeed upregulated by pegIFN-α2b in the liver and can be considered bona fide candidate antiviral effector genes. However, IRF1, IRF2, and IRF7 are transcription factors, and IFIH1 (MDA5), RIGI, IFIT3, and TRIM14 are involved in sensory pathways that activate IFN-β in infected cells (41–43). These seven ISGs are most likely not direct-acting antiviral effector proteins. IFITM1 has been recently shown to be a tight-junction protein expressed in hepatocytes and has been found to inhibit HCV entry (44). IFITM3 is an important restriction factor for the influenza virus and also acts through inhibition of cell entry (45). PLSCR1 restricts RNA viruses, probably by enhancing the induction of a subset of ISGs including IFIT1 and IFIT2, two antiviral effectors that inhibit translation at the ribosome by binding to eIF3 (46). Finally, RNaseL is a nonspecific antiviral effector that degrades viral and host RNAs upon activation by 2′-5′oligoadenylates (2). Based on their proven direct antiviral effector functions, their

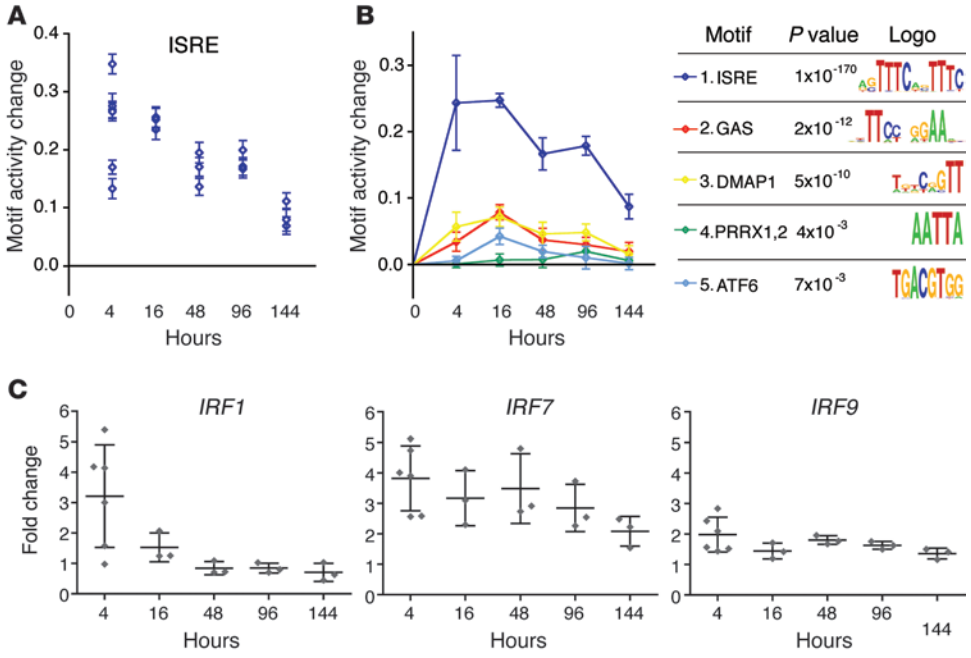

Figure 6
MARA reveals ISRE as the most significantly upregulated motif. (**A**) Activity changes of the ISRE motif in each patient, as inferred by MARA, showed a significant increase in ISRE activity for every patient at every time point. Shown are inferred activity changes (points) ± 1 SD (bars). (**B**) Motif activity profiles of the top five motifs with the most significant positive activity changes. Shown are the mean activity changes per time point (lines) ± 1 SEM as well as the *P* values and sequence logos of the motifs. (**C**) Fold change of *IRF1*, *IRF7*, and *IRF9* mRNA expression for every patient. Shown are the mean values with SEM at each time point.

identification in the above-mentioned siRNA interference and overexpression screens (39, 40), and their pegIFN-α2b–induced upregulation in the liver, IFITM1, IFITM3, PLSCR1, and RNaseL are prime candidates for anti-HCV effectors in humans. Most likely, however, many more of the upregulated ISGs are involved in an orchestrated antiviral effector program that can eliminate HCV from chronically infected patients.

On a more fundamental level, our study also provides for the first time important insights into how IFN-α regulates gene induction over a prolonged observation period of 1 week. Our analysis of global gene expression data obtained from biopsies performed at five time points up to 6 days after pegIFN-α2b injection with an unbiased mathematical model, using an infinite Gaussian mixture model with a Dirichlet process prior, produced four robust clusters of upregulated ISGs with distinct kinetic patterns. Surprisingly, the ISRE promoter element was by far the most important TFBS motif in all the clusters. This clearly demonstrates that ISGs with late or delayed maximal expression are not induced by a different set of transcription factors that could be upregulated by the primary IFN-α–induced transcription factors ISGF3 and STAT1 homodimers and that could then stimulate a second (and third) wave of gene transcription. Based on our nuclear run-on assays and mRNA decay rate measurements in cell culture experiments, we propose that a different duration of gene transcription as well as a different mRNA stability are responsible for the distinct kinetic expression profiles of ISG clusters.

We examined the relative contribution of transcription factor–binding motifs to the global gene expression by MARA, which revealed ISRE to be the most significantly changing motif across all time points up to 6 days. ISRE motifs are the binding sites for ISGF3 and also IRFs. ISGF3 is activated by IFN-α–induced phosphorylation of STAT1 and STAT2. In hepatocytes, signaling through the Jak/STAT pathway becomes refractory within the first day after injection. We observed that the ISRE motif activity indeed peaked at the 4-hour and 16-hour time points, but remained increased even at later time points (Figure 6B). The persistent activation of ISRE sites might be caused by ongoing activation of ISGF3 in hepatocytes at lower levels that are not readily detectable by p-STAT1 immunoblotting. Alternatively, it might reflect the persistent activation of the Jak/STAT pathway in nonparenchymal cells that do not become refractory. Persistent ISRE motif activity could also be driven by IRF7. *IRF7* mRNA was induced during the entire 1-week dosing interval of pegIFN-α (Figure 6C), and it is likely that IRF7 protein was upregulated as well. However, the transcriptional activity of IRF7 is tightly regulated by serine phosphorylation by IKK-α, a downstream component of cellular sensory pathways that are activated by viral PAMPs (23, 24, 47, 48). IRF7-mediated gene induction would occur only in HCV-infected cells. The strong upregulation of *IFI27* mRNA in more than 90% of hepatocytes at the 96-hour time point (Figure 2A) is not likely to be caused by activated IRF7, because HCV rarely infects more than 50% of hepatocytes (49), although we cannot rule out an alternative activation of IRF7 in uninfected cells in the context of IFN treatment.

Finally, our work also sheds light on the role of U-STAT1 as a transcriptional activator that has been proposed to be important in prolonging IFN-α–induced gene transcription. We hypothesized that U-STAT1 target genes would also be strongly expressed at later time points during the 1-week pegIFN-α2b dosing interval, because U-STAT1 was indeed strongly upregulated during the entire week after pegIFN-α2b injection, whereas STAT1 phosphorylation occurred only during the first day. However, the U-STAT1 target genes identified by Cheon and Stark (25) had expression kinetics not different from other p-STAT1–driven ISGs. We therefore addressed the transcriptional activity of U-STAT1 on a STAT1-null background by expressing a mutant tyrosine 701 full-length STAT1 in U3A cells that lack STAT1. Despite very high expression levels, U-STAT1 did not induce ISGs in these cells. We conclude that in cells that lack a WT STAT1, U-STAT1 cannot induce ISG transcription. These findings do not support a role

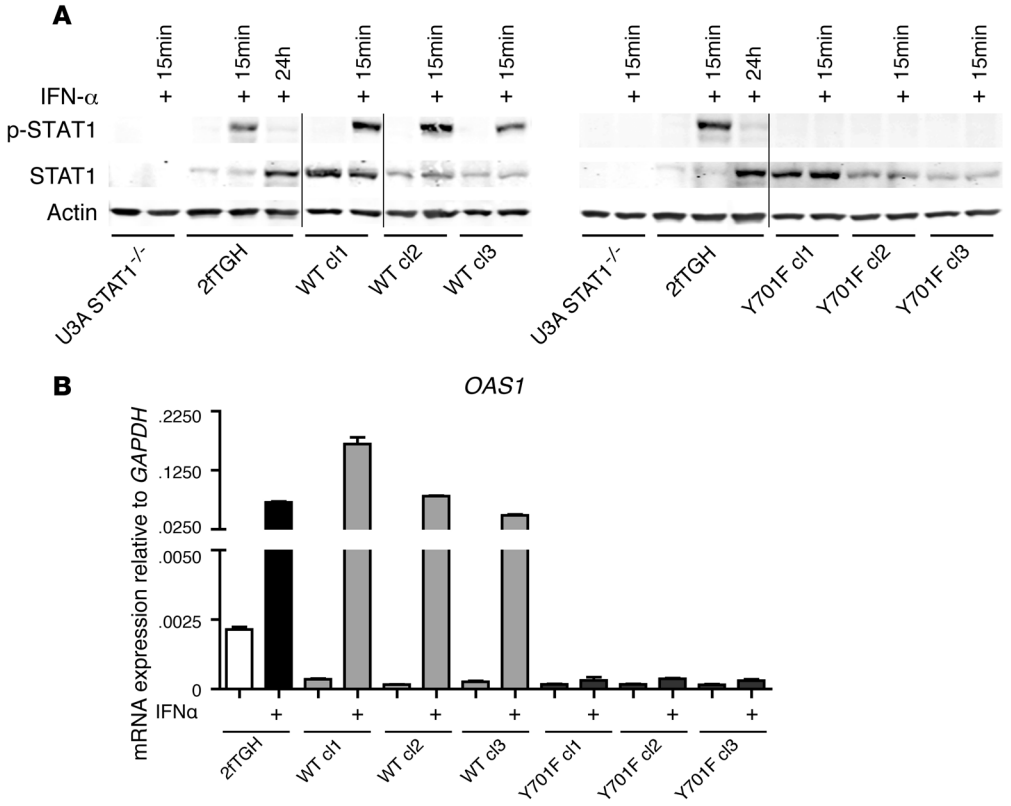

Figure 7

U-STAT1 does not induce ISGs. (**A**) Three clones with different expression levels of WT (WT cl1, WT cl2, and WT cl3) or mutated STAT1 (Y701F cl1, Y701F cl2, and Y701F cl3) were stimulated with IFN-α. STAT1-deficient U3A cells and STAT1 WT parental 2fTGH cells were used as controls. IFN-α induced STAT1 phosphorylation in 2fTGH and in all three WT clones. Actin is shown as a loading control. The cells were either untreated or treated for 15 minutes with 1,000 U/ml of IFN-α. WT cl1 and Y701F cl1 express STAT1 in an amount similar to that induced by 2fTGH cells treated for 24 hours with 1,000 U/ml of IFN-α. Shown are representative blots each from three independently performed experiments (black lanes separate blots that were derived from the same gel, but were noncontiguous). (**B**) IFN-α–induced *OAS1* mRNA expression relative to *GAPDH* was assessed by qRT-PCR. Cells were treated with 1,000 U/ml IFN-α for 8 hours. Upregulation of OAS1 was found only in cells with WT STAT1 after IFN-α treatment. Expression of maximal amounts of Y701F-mutated STAT1 in U3A cells did not induce ISG expression. Shown are the mean values with SEM of three replicate experiments.

for U-STAT1 in prolonging pegIFN-α–induced gene transcription in the liver. Nevertheless, we would like to point out that these findings might be specific for U3A cells, and therefore we cannot formally exclude that U-STAT1 is driving gene transcription in human hepatocytes.

In conclusion, pegIFN-α induces a transient activation of Jak/STAT signaling in hepatocytes that is terminated by the prolonged upregulation of USP18. The predominant transcription factor is ISGF3. Hundreds of genes were induced and can be classified into four robust clusters with distinct kinetic expression patterns. ISGs with peak expression levels at later time points were not induced by secondary transcription factors, and we could not substantiate a role for U-STAT1 in prolonged ISG induction. Our data do not support the prevailing explanation for the superior antiviral efficacy of pegylated versus conventional IFN-α, i.e., that the constantly high serum levels of pegIFN-α cause permanent stimulation of the IFN signal transduction pathways and prolonged IFN-stimulated gene expression in infected hepatocytes. Rather, we found that pegIFN-α induced a broader range of genes, including many genes involved in cellular immune responses. The prolonged serum half-life of pegIFN-α permits a continuous stimulation of nonparenchymal cells in the liver which, contrary to hepatocytes, do not become refractory, but remain sensitive to pegIFN-α during the entire 1-week dosing interval. We therefore propose that the superior efficacy of pegIFN-α is caused by an indirect mechanism involving infiltrating or liver-resident immune cells.

Methods

Patients. The patients were recruited between March 2006 and April 2010 at the Hepatology Outpatient Clinic of the University Hospital Basel. Patients with CHC who underwent a biopsy for diagnostic purposes (B1) and provided written informed consent were screened for hepatic ISG expression. The four-gene classifier was used to assess the probability of an SVR (17). Patients with a high probability of achieving an SVR were asked to participate in the study, which included a second biopsy (B2) taken at a particular time point after the first therapeutic injection of pegIFN-α. We included 3 patients for each of the following time points: 16, 48, 96, and 144 hours, and additionally, the analysis included data on 6 patients from a previous study who had a biopsy at 4 hours (patients 1, 2, 6, 7, 8, and 9) (13). The patients received 1.5 μg/kg body weight pegIFN-α2b (Essex Che-

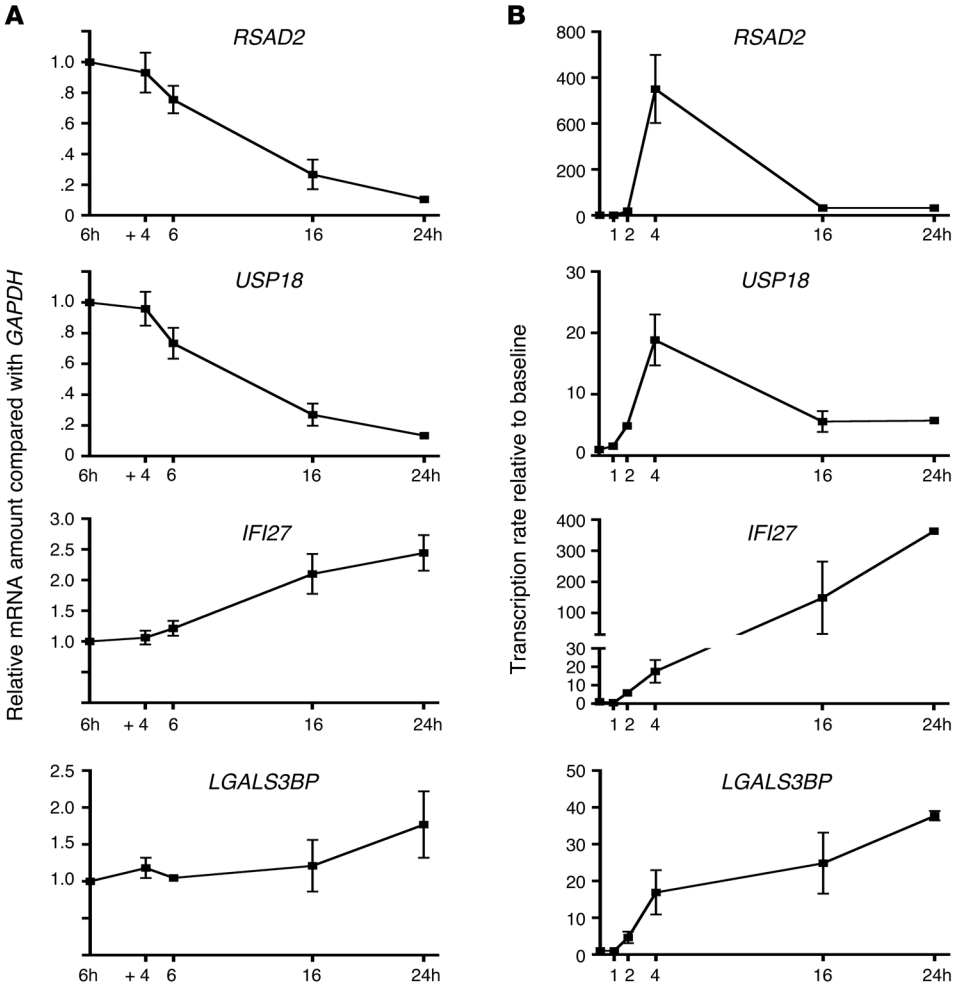

Figure 8
Late ISGs show a more prolonged transcriptional induction and a slower mRNA degradation rate than early ISGs in vitro. (**A**) mRNA degradation of early (*RSAD2*, *USP18*) and late (*IFI27*, *LGALS3BP*) ISGs was assessed in Huh7 after induction with 1,000 U/ml of IFN-α for 6 hours at the indicated time points. Transcription was blocked with actinomycin D, and the mRNA degradation over time was compared with *GAPDH* by qRT-PCR. Results from two independent experiments run in duplicate are shown. (**B**) Transcription rates of early (*RSAD2*, *USP18*) and late (*IFI27*, *LGALS3BP*) ISGs over time in Huh7 cells treated with 1,000 U/ml of IFN-α for the indicated time points. In vitro transcription in isolated nuclei was performed for 45 minutes. Newly transcribed mRNA labeled with biotinylated UTP was isolated and assessed by qRT-PCR. Results depicted as relative transcription compared with untreated baseline are shown from two independent experiments run in duplicate.

mie). Weight-adjusted ribavirin treatment was initiated only after the second biopsy to avoid confounding effects. An additional 3 patients treated with 180 μg of pegIFNα-2a (Roche) were included for the 144-hour time point study. Blood for serum analysis was taken at the time of the first and second biopsies. Serum HCV RNA was quantified using the COBAS AmpliPrep/COBAS TaqMan HCV Test and the COBAS AMPLICOR Monitor (Roche Molecular Systems).

Details regarding the 6 patients treated with IFN-α2a have been described previously (18). The patients included in the present analysis correspond to patients 2–7 in the original publication (18).

IL28B genotyping. DNA extraction and genotyping for the single nucleotide polymorphism rs12979860 near the *IL28B* gene were performed as described previously (17).

Measurement of serum proteins. Serum was collected before the first injection of pegIFN-α and at the time of the second biopsy. Serum levels of IFN-α2b and pegIFN-α2a were measured with an ELISA kit (Verikine 41100; PBL InterferonSource). Standard curves were prepared separately for pegIFN-α2a and -2b by a serial dilution starting at 12.5 pg/ml. The patient serum samples were diluted 10 times in sample diluent. IP-10 serum levels were measured with an ELISA (BD OptEIA Set Human IP-10, 2732KI; BD Biosciences) according to the manufacturer's instructions.

IHC. Four-micrometer-thick serial sections were cut from formalin-fixed, paraffin-embedded liver biopsy specimens, rehydrated, pretreated for 20 minutes in ER2 solution, incubated with a monoclonal rabbit antibody against p-STAT1 (dilution 1:200, no. 9167; Cell Signaling Technology) or USP18 (1:100, catalog 4813; Cell Signaling Technology), and counterstained with hematoxylin. Standard indirect immunoperoxidase procedures were used for IHC (ABC-Elite; Vectra Laboratories). The staining procedure was performed with an automated stainer (Bond; Vision BioSystems).

RNA extraction and microarray hybridization. Total RNA was extracted from human liver tissue using QIAzol reagent and the RNeasy Mini Kit (QIAGEN) according to the manufacturer's instructions. Gene expression was assessed by microarray analysis using Affymetrix Human Genome U133 Plus 2.0 arrays. Total RNA (1 μg) from each sample was reverse transcribed using a Genechip 3'IVT Express Kit (Affymetrix) according to the manufacturer's instructions. The Hybridization and Wash Kit (Affymetrix) was used to hybridize the samples. All original array data are deposited in the NCBI's Gene Expression Omnibus (GEO GSE48445).

RNA ISH. For the present study, we adapted a highly sensitive and specific ISH system (QuantiGene ViewRNA; Affymetrix). OCT-embedded and shock-frozen biopsies were cryosectioned (10-μm-thick sections) in a cryostat and mounted on Superfrost Plus Gold glass slides (Thermo Fisher Scientific). Upon fixation (4% formaldehyde, 16–18 hours at 4°C), washing, and dehydration in ethanol, the sections were pretreated by boiling for 1 minute in Pretreatment Solution, followed by a 10-minute digestion in Protease QF (both from Affymetrix). Sections were hybridized for 2 hours at 40°C with QuantiGene ViewRNA probes against *MX1*, *IFI27*, *SOCS1*, and *PDL1* (Affymetrix). Bound probes were preamplified and subsequently

amplified according to the manufacturer's instructions. Labeled oligonucleotide probes conjugated with alkaline phosphatase (LP-AP) type 1 or type 6 were added, followed by the addition of fast red or fast blue substrate used to detect ISG mRNAs. Finally, the slides were counterstained with Meyer's hematoxylin and embedded with DAPI-containing aqueous mounting medium (Roti-Mount FluorCare DAPI; Roth). Random images were acquired using a laser scanning confocal microscope (LSM710; Zeiss) and Zen2 software (Zeiss). All images were acquired with identical settings and saved in the Zeiss confocal file format (.lsm).

MARA. Here, we provide a brief description of MARA and its particular use in this work. For a detailed description of the general approach, the reader is referred to the FANTOM Consortium study (21).

To model the activity $A_{m,s}$ of a motif m in sample s, MARA uses a simple linear model that relates the number of binding sites $N_{p,m}$ in promoter p, for each of a large number of regulatory motifs m, to the expression $E_{p,s}$ of promoter p in samples:

$$E_{p,s} = \tilde{c}_s + c_p + \sum_m N_{p,m} A_{m,s} \quad \text{(Equation 1)}$$

where c_s represents the mean expression in sample s, and c_p is the basal expression of promoter p. To determine promoter expression levels, we first computed the transcript expression levels by averaging weighted probeset signals (preprocessed as described above) over all probesets that matched a particular transcript as annotated by Affymetrix (Affymetrix annotation, Release 31 [NM accession RefSeqs only]). In this averaging, a probeset's signal was weighted by the number of transcripts it matches. Subsequently, transcript expression levels were mapped to the human promoterome by averaging the weighted expression levels over all transcripts associated with a particular promoter. In this averaging, each transcript's signal was weighted by the inverse of the number of promoters that express this particular transcript. To predict the TFBSs in each promoter, we used a curated set of transcription factor–binding motifs from SwissRegulon (50) with minor changes: since the SwissRegulon IRF1,2,7 motif only covered the IRF core consensus sequence, we replaced it with the ISRE (ThioMac-LPS-exp) motif to better cover the ISGF3 and IRF9 binding sites in our analysis. In addition, we replaced the three highly redundant STAT motifs from SwissRegulon with a single, high-quality GAS motif (HelaS3-STAT1-ChIP-Seq, as the GAS motif representative). Both motifs were obtained with HOMER software (22). By applying MARA, we obtained for every motif m in each sample s an expected activity $A_{m,s}$ and a corresponding error $\delta_{m,s}$.

Determining donor-specific motif activity changes due to IFN-α treatment. For every donor and every motif m, we calculated the difference between the motif activity before IFN-α treatment ($A^b{}_m$) and the motif activity after IFN-α treatment: ($A^a{}_m$)

$$A^{\Delta}_m = A^a_m - A^b_m \quad \text{(Equation 2)}$$

as well as the corresponding SD:

$$\sigma^{\Delta}_m = \sqrt{(\sigma^a_m)^2 + (\sigma^b_m)^2}. \quad \text{(Equation 3)}$$

Thus, for every motif m and each donor d, the expression data D imply an expected activity change $A^{\Delta}_{m,d}$ with corresponding SD $\sigma^{\Delta}_{m,d}$. Consequently, the probability of the data D, assuming a true (unobserved) activity change $\tilde{A}^{\Delta}_{m,d}$, is a Gaussian with the expected mean $A^{\Delta}_{m,d}$ and SD $\sigma^{\Delta}_{m,d}$:

$$P\left(D|\tilde{A}^{\Delta}_{m,d}\right) = \frac{1}{\sqrt{2\pi}\sigma^{\Delta}_{m,d}} \exp\left[-\frac{1}{2}\frac{\left(\tilde{A}^{\Delta}_{m,d} - A^{\Delta}_{m,d}\right)^2}{(\sigma^{\Delta}_{m,d})^2}\right] \quad \text{(Equation 4)}$$

where $\tilde{A}^{\Delta}_{m,d}$ is the true (unobserved) activity change.

Determining mean motif activity changes due to pegIFN-α treatment at certain time points. To obtain mean activity changes for every group of donors $g \in G$ whose second biopsy was taken at an equal time point after pegIFN-α treatment, we assumed that the activity changes A^{Δ}_m of motif m were Gaussian distributed (with mean $A^{\Delta}_{m,g}$ and variance $(\sigma^{\Delta}_{m,d})^2$). Accordingly, the probability of an activity change $\tilde{A}^{\Delta}_{m,d}$ in donor d is:

$$P\left(\tilde{A}^{\Delta}_{m,d}|A^{\Delta}_{m,g}, \sigma^{\Delta}_{m,g}\right) = \frac{1}{\sqrt{2\pi}\sigma^{\Delta}_{m,g}} \exp\left[-\frac{1}{2}\frac{\left(\tilde{A}^{\Delta}_{m,d} - A^{\Delta}_{m,g}\right)^2}{(\sigma^{\Delta}_{m,g})^2}\right] \quad \text{(Equation 5)}$$

For each donor $d \in g$, we combine Equations 4 and 5 and integrate out all unknown (true activity changes) $\tilde{A}^{\Delta}_{m,d}$ so that we can calculate the probability of the data D given the mean activity of the group $A^{\Delta}_{m,g}$ and the corresponding error $\sigma^{\Delta}_{m,g}$:

$$P(D|A^{\Delta}_{m,g}, \sigma^{\Delta}_{m,g}) = \prod_{d \in G}\left[\int d\tilde{A}^{\Delta}_{m,d} P(D|\tilde{A}^{\Delta}_{m,d}) P(\tilde{A}^{\Delta}_{m,d}|A^{\Delta}_{m,g}, \sigma^{\Delta}_{m,g})\right] \quad \text{(Equation 6)}$$

Solving these integrals analytically gives:

$$P(D|A^{\Delta}_{m,g}, \sigma^{\Delta}_{m,g}) = \prod_{d \in g} \frac{1}{\sqrt{2\pi((\sigma^{\Delta}_{m,g})^2 + (\sigma^{\Delta}_{m,d})^2)}} \exp\left[-\frac{(A^{\Delta}_{m,d} - A^{\Delta}_{m,g})^2}{2((\sigma^{\Delta}_{m,g})^2 + (\sigma^{\Delta}_{m,d})^2)}\right] \quad \text{(Equation 7)}$$

We then numerically determine the value $\sigma^{\Delta*}_{m,g}$ that maximizes Equation 7. Assuming a uniform prior for $A^{\Delta}_{m,g}$, we obtain an expression for the posterior probability $P(A^{\Delta}_{m,g}|D)$, which is a Gaussian with mean

$$\bar{A}^{\Delta}_{m,g} = \frac{\sum_{d \in g} \frac{A^{\Delta}_{m,d}}{(\sigma^{\Delta*}_{m,g})^2 + (\sigma^{\Delta}_{m,d})^2}}{\sum_{d \in g} \frac{1}{(\sigma^{\Delta*}_{m,g})^2 + (\sigma^{\Delta}_{m,d})^2}}, \quad \text{(Equation 8)}$$

and SEM

$$\bar{\sigma}^{\Delta}_{m,g} = \sqrt{\frac{1}{\sum_{d \in g} \frac{1}{(\sigma^{\Delta*}_{m,g})^2 + (\sigma^{\Delta}_{m,d})^2}}} \quad \text{(Equation 9)}$$

where $\sigma^{\Delta*}_{m,g}$ is the maximum likelihood estimate of Equation 7. We call $A^{-\Delta}_{m,g}$ the mean activity change for group g and $\sigma^{-\Delta}_{m,g}$ the corresponding SEM. To obtain a measure for the significance of the mean activity change for group g, we calculate a corresponding z value:

$$\bar{Z}^{\Delta}_{m,g} = \sqrt{\frac{\bar{A}^{\Delta}_{m,g}}{\bar{\sigma}^{\Delta}_{m,g}}}. \quad \text{(Equation 10)}$$

Finally, a global z value considering all time points is given by:

$$\bar{Z}^{\Delta}_{m} = \sqrt{\frac{\sum_{g \in G} (\bar{z}^{\Delta}_{m,g})^2}{|G|}}. \quad \text{(Equation 11)}$$

To calculate a P value for the calculated z value $\bar{z}^{\Delta}_{m}$, we used the null hypothesis that the z statistic $\bar{z}^{\Delta}_{m}$ in each group g, i.e., the ratio between the motif

activity change and its standard error was drawn from a Gaussian with mean zero and variance 1. Under this null hypothesis, the distribution of the statistic,

$$\left(\bar{z}_m^{\Delta}\right)^2 * G = \sum_{g=1}^{G} \left(\bar{z}_{m,g}^{\Delta}\right)^2 \qquad \text{(Equation 12)}$$

with G representing the number of groups (wherein each group represents a time point), is gamma distributed, and we used this distribution to calculate the P value corresponding to the z value of each of our motifs.

TFBS analysis. TFBS analysis was carried out using HOMER software (22) (http://biowhat.ucsd.edu/homer/motif/index.html). Briefly, promoter regions (2 kbp upstream and 500 bp downstream of the transcription start site) of all genes within each cluster were screened for known TFBS. Enrichment of TFBS in our gene lists relative to all human promoter regions was assessed by hypergeometric tests.

Quantitative real-time RT-PCR. RNA was reverse transcribed by Moloney murine leukemia virus reverse transcriptase (Promega) in the presence of random primers (Promega) and deoxynucleoside triphosphate. The samples were incubated for 5 minutes at 70°C and then for 1 hour at 37°C. The reaction was stopped by heating at 95°C for 5 minutes. SYBR real-time PCR was performed using the SYBR Green PCR Master Mix (Applied Biosystems). Intron-spanning primers for *GAPDH*, *HERC6, IFI27*, *IFI44L*, *ISG15*, *LGALS3BP*, *MX1*, *OAS1*, *OAS2*, *RSAD2*, and *USP18* were used (Supplemental Table 5). All reactions were performed in duplicate on an ABI 7500 Real-Time PCR System (Applied Biosystems). mRNA expression levels of the transcripts were normalized to *GAPDH* using the ΔCt method.

Western blot analysis. Whole-cell extracts and blotting of human liver samples and cells were performed as described (13). The membranes were incubated with primary antibodies against p-STAT1 (1:1,000, catalog 9171; Cell Signaling Technology), STAT1 (1:1,000, catalog 610116; BD Transduction Laboratories), USP18 (1:1,000, no. 4813; Cell Signaling Technology), and β-actin (1:2,000, A5441; Sigma-Aldrich) diluted in Tris-buffered saline containing Tween-20 (TBST) overnight at 4°C. After three washes with TBST, membranes were incubated for 1 hour at room temperature with fluorescent secondary goat anti-mouse (IRDye 680) or anti-rabbit (IRDye 800) antibodies (both from LI-COR Biosciences). Blots were scanned using the Odyssey Infrared Imaging System (LI-COR Biosciences).

Cell culture. Huh7 cells were maintained in DMEM (Gibco) supplemented with 10% FBS. 2fTGH and U3A STAT1$^{-/-}$ cells were maintained in DMEM with 10% FBS and 250 μg/ml of hygromycin B (Sigma-Aldrich). The stably transfected U3A STAT1$^{-/-}$ cells were selected with 800 μg/ml of G418 (catalog 345810; Calbiochem). Cells were treated with 1,000 U/ml human IFN-α (Roferon; Roche) and/or with 5 μg/ml actinomycin D (Sigma-Aldrich).

Site-directed mutagenesis and transfection. The STAT1-flag-pcDNA3 (STAT1-WT) was provided by J.E. Darnell (Rockefeller University, New York City, New York, USA). STAT1 (Y701F)-flag-pcDNA3 was generated from STAT1-flag-pcDNA3 using the method described by Mikaelian and Sergeant (51). Briefly, two consecutive PCR reactions with 30 cycles were performed using 20 ng of template DNA, 200 μM dNTP, 1 U of *Pfu* DNA polymerase (Promega), and 5 μM of each of the following primers: 5′-CTGGCACCAGAACGAATGA-3′; 5′-ATTTAGGTGACACTATAG-3′; 5′-GGAACTGGATTCATCAAGACTGAG-3′; and 5′-CTCAGTCTTGATGAATCCAGTTC-3′, in a final volume of 25 μl. The amplified products were loaded on a 1.5% agarose gel, excised, digested by BlpI and ApaI, and ligated into STAT1-flag-pcDNA3, previously cut with the same restriction enzymes. Mutation of Tyr701 to Phe was confirmed by sequencing.

U3A STAT1$^{-/-}$ cells were transfected with 1 μg of the respective plasmid using Fugene HD (Roche) according to the manufacturer's instructions. Cells were selected with 800 μg/ml of hygromycin B (Roche) for 15 days, and single clones were chosen.

Nuclear run-on assay. After IFN-α treatment, cells were washed with 1× PBS, treated with 0.25% trypsin for 4 minutes (Gibco), suspended in 10 ml of ice-cold diethylpyrocarbonate-treated (DEPC-treated) 1× PBS, and concentrated by centrifugation (160 *g*, 10 minutes). Cells were then washed once with ice-cold buffer 1 containing 10 mM Tris-HCl (pH 7.4), 150 mM KCl, and 8 mM Mg acetate, centrifuged at 530 *g* for 10 minutes, and subsequently lysed with buffer 1 with the addition of 0.5% Igepal (Sigma-Aldrich) for 10 minutes at 4°C. Nuclei were then isolated by a sucrose gradient (600 mM), then washed and suspended in buffer containing 40% glycerol. Nuclei were immediately used for the run-on assay. Nuclei (5×10^6) were incubated in reaction buffer containing 5 mM Tris-HCl (pH 8.0), 2.5 mM $MgCl_2$, 150 mM KCl, and 2.5 mM each of ATP, GTP, CTP, UTP, and biotin-16-UTP (Roche) for 45 minutes at 30°C. RNA was then isolated with TRIzol according to the manufacturer's instructions. Subsequently, biotinylated RNA was purified with streptavidin-coupled beads (Dynabeads M-280; Invitrogen) according to the manufacturer's instructions, and RNA was again isolated with TRIzol.

Statistics. Microarray analysis was performed with Bioconductor packages within the R statistical environment (52). Data were preprocessed using the standard RMA algorithm. Batch effects observed between the human liver samples that were processed and hybridized at different times were corrected using the ComBat algorithm (53). Probesets with very low expression intensities (below 80 in the highest-expressing sample) as well as the control probesets were excluded from the subsequent analyses. The list of significantly regulated probesets was compiled as follows: (a) probesets showing more than a 2-fold difference in levels between the B1 and B2 samples taken from the same patient were selected; (b) for every time point, the probesets that changed in two-thirds of the patients were retained. Probesets fulfilling those criteria were included in the clustering analysis. The expression data were normalized so that total expression levels did not affect the grouping of the probesets. An infinite Gaussian mixture model with a Dirichlet process prior was used to produce the gene clusters. This nonparametric model suggests a growing number of Gaussians to describe the gene expressions. With the special choice of a Dirichlet process prior, the number of clusters need not be fixed in advance, but is adaptively chosen based on the observed data. The results were tested for robustness by moderately changing the hyperparameters that control the Dirichlet process.

Enrichment of Kyoto Encyclopedia of Genes and Genomes (KEGG) pathways and GO biological process terms were assessed using DAVID software, version 6.7. Additional statistical analyses using a 2-tailed Student's t test were carried out using GraphPad Prism software, version 6.0 (GraphPad Software). A P value of less than 0.05 was considered significant.

Study approval. All patients provided written informed consent to participate in the study, which was approved by the ethics committee of Basel.

Acknowledgments

We thank the patients who donated liver biopsy specimens for this study. We are grateful to François H.T. Duong for helpful discussions and Philippe Demougin (Life Sciences Training Facility, Pharmazentrum, Basel, Switzerland) for providing technical help with the processing of microarrays. We also thank Sylvia Ketterer for excellent technical assistance.

This work was supported by Swiss National Science Foundation (SNF) grant 320030-130243 (to M.H. Heim) and SNF grant 323500-123714 (to M.T. Dill). A.J. Gruber was supported by a Fellowship of the Werner Siemens-Foundation.

Received for publication April 9, 2013, and accepted in revised form December 17, 2013.

Address correspondence to: Markus H. Heim, University of Basel, Department of Biomedicine, Zentrum für Lehre und Forschung, Hebelstrasse 20, 4031 Basel, Switzerland. Phone: 41.61.265.33.62; Fax: 41.61.265.38.47; E-mail: markus.heim@unibas.ch.

1. Stetson DB, Medzhitov R. Type I interferons in host defense. *Immunity*. 2006;25(3):373–381.
2. Sadler AJ, Williams BR. Interferon-inducible antiviral effectors. *Nat Rev Immunol*. 2008;8(7):559–568.
3. Darnell JE, Darnell JE Jr, Kerr IM, Stark GR. Jak-STAT pathways and transcriptional activation in response to IFNs and other extracellular signaling proteins. *Science*. 1994;264(5164):1415–1421.
4. Song MM, Shuai K. The suppressor of cytokine signaling (SOCS) 1 and SOCS3 but not SOCS2 proteins inhibit interferon-mediated antiviral and antiproliferative activities. *J Biol Chem*. 1998; 273(52):35056–35062.
5. Larner AC, Chaudhuri A, Darnell JE, Darnell JE Jr. Transcriptional induction by interferon. New protein(s) determine the extent and length of the induction. *J Biol Chem*. 1986;261(1):453–459.
6. Sarasin-Filipowicz M, et al. α Interferon induces long-lasting refractoriness of JAK-STAT signaling in the mouse liver through induction of USP18/UBP43. *Mol Cell Biol*. 2009;29(17):4841–4851.
7. Hoofnagle JH, et al. Treatment of chronic non-A, non-B hepatitis with recombinant human α interferon. A preliminary report. *N Engl J Med*. 1986;315(25):1575–1578.
8. Lauer GM, Walker BD. Hepatitis C virus infection. *N Engl J Med*. 2001;345(1):41–52.
9. Fried MW, et al. Peginterferon alfa-2a plus ribavirin for chronic hepatitis C virus infection. *N Engl J Med*. 2002;347(13):975–982.
10. Manns MP, et al. Peginterferon alfa-2b plus ribavirin compared with interferon alfa-2b plus ribavirin for initial treatment of chronic hepatitis C: a randomised trial. *Lancet*. 2001;358(9286):958–965.
11. Zeuzem S, et al. Peginterferon alfa-2a in patients with chronic hepatitis C. *N Engl J Med*. 2000; 343(23):1666–1672.
12. Lindsay KL, et al. A randomized, double-blind trial comparing pegylated interferon alfa-2b to interferon alfa-2b as initial treatment for chronic hepatitis C. *Hepatology*. 2001;34(2):395–403.
13. Sarasin-Filipowicz M, et al. Interferon signaling and treatment outcome in chronic hepatitis C. *Proc Natl Acad Sci U S A*. 2008;105(19):7034–7039.
14. Chen L, et al. Hepatic gene expression discriminates responders and nonresponders in treatment of chronic hepatitis C viral infection. *Gastroenterology*. 2005;128(5):1437–1444.
15. Asselah T, et al. Liver gene expression signature to predict response to pegylated interferon plus ribavirin combination therapy in patients with chronic hepatitis C. *Gut*. 2008;57(4):516–524.
16. Feld JJ, et al. Hepatic gene expression during treatment with peginterferon and ribavirin: Identifying molecular pathways for treatment response. *Hepatology*. 2007;46(5):1548–1563.
17. Dill MT, et al. Interferon-induced gene expression is a stronger predictor of treatment response than IL28B genotype in patients with hepatitis C. *Gastroenterology*. 2011;140(3):1021–1031.
18. Lau DT, et al. Innate immune tolerance and the role of kupffer cells in differential responses to interferon therapy among patients with HCV genotype 1 infection. *Gastroenterology*. 2013;144(2):402–413.
19. Foster GR. Pegylated interferons for the treatment of chronic hepatitis C: pharmacological and clinical differences between peginterferon-alpha-2a and peginterferon-alpha-2b. *Drugs*. 2010; 70(2):147–165.
20. Silva M, et al. A randomised trial to compare the pharmacokinetic, pharmacodynamic, and antiviral effects of peginterferon alfa-2b and peginterferon alfa-2a in patients with chronic hepatitis C (COMPARE). *J Hepatol*. 2006;45(2):204–213.
21. Consortium F, et al. The transcriptional network that controls growth arrest and differentiation in a human myeloid leukemia cell line. *Nat Genet*. 2009; 41(5):553–562.
22. Heinz S, et al. Simple combinations of lineage-determining transcription factors prime cis-regulatory elements required for macrophage and B cell identities. *Mol Cell*. 2010;38(4):576–589.
23. Tamura T, Yanai H, Savitsky D, Taniguchi T. The IRF family transcription factors in immunity and oncogenesis. *Annu Rev Immunol*. 2008;26:535–584.
24. Hoshino K, et al. IkappaB kinase-alpha is critical for interferon-alpha production induced by Toll-like receptors 7 and 9. *Nature*. 2006; 440(7086):949–953.
25. Cheon H, Stark GR. Unphosphorylated STAT1 prolongs the expression of interferon-induced immune regulatory genes. *Proc Natl Acad Sci U S A*. 2009; 106(23):9373–9378.
26. Muller M, et al. Complementation of a mutant cell line: central role of the 91 kDa polypeptide of ISGF3 in the interferon-alpha and -gamma signal transduction pathways. *EMBO J*. 1993; 12(11):4221–4228.
27. Hao S, Baltimore D. The stability of mRNA influences the temporal order of the induction of genes encoding inflammatory molecules. *Nat Immunol*. 2009;10(3):281–288.
28. Wu X, Brewer G. The regulation of mRNA stability in mammalian cells: 2.0. *Gene*. 2012;500(1):10–21.
29. Cramp ME, Rossol S, Chokshi S, Carucci P, Williams R, Naoumov NV. Hepatitis C virus-specific T-cell reactivity during interferon and ribavirin treatment in chronic hepatitis C. *Gastroenterology*. 2000;118(2):346–355.
30. Kamal SM, Fehr J, Roesler B, Peters T, Rasenack JW. Peginterferon alone or with ribavirin enhances HCV-specific CD4 T-helper 1 responses in patients with chronic hepatitis C. *Gastroenterology*. 2002;123(4):1070–1083.
31. Claassen MA, de Knegt RJ, Turgut D, Groothuismink ZM, Janssen HL, Boonstra A. Negative regulation of hepatitis C virus specific immunity is highly heterogeneous and modulated by pegylated interferon-alpha/ribavirin therapy. *PLoS One*. 2012; 7(11):e49389.
32. Barnes E, et al. The dynamics of T-lymphocyte responses during combination therapy for chronic hepatitis C virus infection. *Hepatology*. 2002; 36(3):743–754.
33. Aberle JH, et al. $CD4^+$ T cell responses in patients with chronic hepatitis C undergoing peginterferon/ribavirin therapy correlate with faster, but not sustained, viral clearance. *J Infect Dis*. 2007; 195(9):1315–1319.
34. Lanford RE, Guerra B, Lee H, Chavez D, Brasky KM, Bigger CB. Genomic response to interferon-alpha in chimpanzees: implications of rapid downregulation for hepatitis C kinetics. *Hepatology*. 2006;43(5):961–972.
35. Malakhova OA, et al. UBP43 is a novel regulator of interferon signaling independent of its ISG15 isopeptidase activity. *EMBO J*. 2006;25(11):2358–2367.
36. Fenner JE, et al. Suppressor of cytokine signaling 1 regulates the immune response to infection by a unique inhibition of type I interferon activity. *Nat Immunol*. 2006;7(1):33–39.
37. McHutchison JG, et al. Peginterferon alfa-2b or alfa-2a with ribavirin for treatment of hepatitis C infection. *N Engl J Med*. 2009;361(6):580–593.
38. Heim MH. Interferon signaling. In: Clavien PA, Dufour JF, eds. *Signaling Pathways in Liver Diseases*. Berlin, Germany: Springer-Verlag; 2010:189–200.
39. Schoggins JW, et al. A diverse range of gene products are effectors of the type I interferon antiviral response. *Nature*. 2011;472(7344):481–485.
40. Metz P, et al. Identification of type I and type II interferon-induced effectors controlling hepatitis C virus replication. *Hepatology*. 2012; 56(6):2082–2093.
41. Liu XY, Chen W, Wei B, Shan YF, Wang C. IFN-induced TPR protein IFIT3 potentiates antiviral signaling by bridging MAVS and TBK1. *J Immunol*. 2011;187(5):2559–2568.
42. Yoneyama M, et al. Shared and unique functions of the DExD/H-box helicases RIG-I, MDA5, and LGP2 in antiviral innate immunity. *J Immunol*. 2005; 175(5):2851–2858.
43. Versteeg GA, et al. The E3-ligase TRIM family of proteins regulates signaling pathways triggered by innate immune pattern-recognition receptors. *Immunity*. 2013;38(2):384–398.
44. Wilkins C, et al. IFITM1 is a tight junction protein that inhibits hepatitis C virus entry. *Hepatology*. 2013;57(2):461–469.
45. Everitt AR, et al. IFITM3 restricts the morbidity and mortality associated with influenza. *Nature*. 2012; 484(7395):519–523.
46. Terenzi F, Hui DJ, Merrick WC, Sen GC. Distinct induction patterns and functions of two closely related interferon-inducible human genes, ISG54 and ISG56. *J Biol Chem*. 2006;281(45):34064–34071.
47. Marie I, Durbin JE, Levy DE. Differential viral induction of distinct interferon-alpha genes by positive feedback through interferon regulatory factor-7. *EMBO J*. 1998;17(22):6660–6669.
48. Marie I, Smith E, Prakash A, Levy DE. Phosphorylation-induced dimerization of interferon regulatory factor 7 unmasks DNA binding and a bipartite transactivation domain. *Mol Cell Biol*. 2000; 20(23):8803–8814.
49. Wieland S, et al. Simultaneous detection of hepatitis C virus and interferon stimulated gene expression in infected human liver [published online ahead of print October 3, 2013]. *Hepatology*. doi:10.1002/hep.26770.
50. Pachkov M, Balwierz PJ, Arnold P, Ozonov E, van Nimwegen E. SwissRegulon, a database of genome-wide annotations of regulatory sites: recent updates. *Nucleic Acids Res*. 2013; 41(Database issue):D214–D220.
51. Mikaelian I, Sergeant A. A general and fast method to generate multiple site directed mutations. *Nucleic Acids Res*. 1992;20(2):376.
52. R Development Core Team. R: *A Language And Environment For Statistical Computing*. Vienna, Austria: R Foundation for Statistical Computing; 2011.
53. Johnson WE, Li C, Rabinovic A. Adjusting batch effects in microarray expression data using empirical Bayes methods. *Biostatistics*. 2007;8(1):118–127.